SUPPLEMENTARY INFORMATION

Void space control in porous carbon for high density supercapacitive charge storage

Bincy Lathakumary Vijayan[1], Nurul Khairiyyah Mohd Zain[1], Izan Izwan Misnon[1], M. V. Reddy[2], Stefan Adams[3], Chun-Chen Yang[4], Gopinathan M. Anilkumar,[5] and Rajan Jose[1]*

[1]Nanostructured Renewable Energy Materials Laboratory, Faculty of Industrial Sciences & Technology, Universiti Malaysia Pahang, 26300 Kuantan, Malaysia; [2]Centre of Excellence in Transportation Electrification and Energy Storage (CETEES), Hydro-Québec, Varennes, Qc, J3X 1S1, Canada; [3]Department of Materials Science and Engineering, National University of Singapore, Singapore 117576, Singapore; [4]Battery Research Center of Green Energy, Ming Chi University of Technology, New Taipei City, Taiwan; [5] R&D Center, Noritake Co Ltd, 300 Higashiyama, Miyoshi, Aichi 470-0293, Japan;

* Corresponding author. E-mail: rjose@ump.edu.my (Rajan Jose)

The Supplementary Information is divided into three parts: (1) Supplementary Tables, (2) Supplementary Figures, and (3) Supplementary Data. References of the Tables are appended as the last section.

SUPPLEMENTARY INFORMATION

Supplementary Table S1. Summary of various carbon from carbon rich organic precursors for supercapacitor applications

Precursor	Method of synthesis	Surface area ($m^2 g^{-1}$)	Electrolyte	C_S ($F g^{-1}$)	Scan rate/Current density	C_S Retention (%)/ Cycle number	Ref.
Dead Neem leaves	single-step pyrolysis	1230	1 M H_2SO_4	400	0.5 A g^{-1}	NR	[1]
Loofah sponge	KOH activation	2718	6 M KOH	309.6	1 A g^{-1}	81 /10000	[2]
Rapeseed dregs (RDs)	$ZnCl_2$ activation	1417	1 M H_2SO_4	170.5	5 mV s^{-1}	90/6400	[3]
Cladophora glomerata	slow pyrolysis technique	354	3 M KCl	376.7	1 A g^{-1}	92/ 5000	[4]
Tremella	KOH activation	3760	6 M KOH	71	1 A g^{-1}	99/1000	[5]
Stiff silkworm	KOH activation	2523	6 M KOH	304	1 A g^{-1}	95 /4000	[6]
Coconut fiber	Simple one step pyrolysis	7	1.0 M KOH	236	2 mV s^{-1}	100/5000	[7]
Lotus pollens	CO_2 activation	2566	1 M H_2SO_4	244	0.1 A g^{-1}	100/1000	[8]
Sugarcane bagasse	KOH activation	2296	1 M Na_2SO_4	320	0.5 A g^{-1}	93/15000	[9]
Shiitake mushroom	KOH activation	2988	6 M KOH	306	1.0 A g^{-1}	96/15000	[10]

SUPPLEMENTARY INFORMATION

Potato starch & Eucalyptus sawdust	*hydrochar*/ KOH activation	3300	EMImTFSI	160	1 A g^{-1}	90/1000	[11]
Corncob	pyrolysis &KOH activation	3054	6 M KOH	328	0.5 A g^{-1}	91/10000	[12]
Sunflower seed shell	KOH activation	2509	30 wt% KOH	311	250 mA g^{-1}	NR	[13]
Cassava peel waste	KOH activation	1352	0.5 M H_2SO_4	264	NR	NR	[14]
Carrageenan	KOH activation	2502	6 M KOH	230	1 A g^{-1}	95/1000	[15]
Enteromorpha prolifera	self-template method	3332	6 M KOH	210	3 A g^{-1}	NR	[16]
Apricot shell	NaOH activation	2335	6 M KOH	339	50 mA g^{-1}	NR	[17]
Bamboo char	K_2FeO_4 activation	1732	6 M KOH	222	0.5 A g^{-1}	NR	[18]
Bamboo	KOH activation	2221	3 M KOH	293	0.5 A g^{-1}	NR	[19]
Palm kernel shell	KOH activation	462.1	1 M KOH	210	0.5 A g^{-1}	95/1000	[20]
Palm kernel shell	Steam activation	727.3	1 M KOH	123	0.5 A g^{-1}	97/1000	[20]

SUPPLEMENTARY INFORMATION

Palm kernel shell	KOH activation	506.7	1 M Na_2SO_4	150	1 A g^{-1}	97/5000	This work

Supplementary Table S2. Summary of various pseudocapacitive material filled AC for supercapacitor applications. NR stands for "Not Reported".

Composite	Method of synthesis	C_S (F g^{-1})	Potential window (V)	C_S Retention (%)/ Cycle number	Ref.
Macroporous carbon/ MnO_2 nanosheets	Hydrothermal method	386 (1M Na_2SO_4 at 1 A g^{-1})	0.8	83/5000	[21]
CS@MnO_2	Hydrothermal method	178(0.5 M Na_2SO_4 1 A g^{-1})	0.8	NR	[22]
MnO_2/ACFs	Hydrothermal method	135 (1M Na_2SO_4 at 10 mA cm^{-2})	1	99/3000	[23]
Macroporous Mn_2O_3/carbon	*Two-step process*	349 (1 M Na_2SO_4 at 50 mA g^{-1})	0.8	89/2000	[24]
MnO_2/carbon sphere/graphene	*Sonication*	319 (1 M Na_2SO_4 at 1 A g^{-1})	0.8	94/5000	[25]
MnO_2/C	*Direct reaction*	328 (1 M Na_2SO_4 at 0.5 A g^{-1})	1	88/4000	[26]
Carbon nanotube@ manganese oxide nanosheet	*Seeded growth*	298 (0.5 M Na_2SO_4 at 0.5 A g^{-1})	0.8	90/5000	[27]
MnO_2/RHC	*in -situ chemical precipitation*	210 (0.5 M Na_2SO_4 at 0.5 A g^{-1})	1	80/5000	[28]
3D Ni/CNTs	ED-CVD method	175(1 M Na_2SO_4 at 5 A g^{-1})	1	99/10000	[29]
10 wt.% Mn_2O_3@AC	*KOH activation*	350 (1 M Na_2SO_4 at 1 A g^{-1})	1.2	97/5000	[30]
$ZnMn_2O_4$-CNT	hydrothermal method	103 (1 M Na_2SO_4 at 0.1 A g^{-1})	0.8	85/1000	[31]
Manganese oxide nanoneedle/carbide-derived carbon (MnO_2/CDC)	hydrothermal	255.8 (1 M Na_2SO_4 at 1 A g^{-1})	0.7	85.5/2000	[32]
RGO/porous carbon/MnO_2	electrodeposition method	135 (1M Na_2SO_4 at1mA cm^{-2})	1	85/5000	[33]
Mn_2O_3/carbon	Calcination	776(1 M Na_2SO_4 at	0.8	100/3000	[34]

SUPPLEMENTARY INFORMATION

		1 A g^{-1})			
$NiCo_2O_4$ embedded carbon fiber	chemical bath deposition	1925 (2 M KOH at 1 A g^{-1})	0.45	87/5000	[35]
SiO2@C-NCS nanocomposite	Solution based method	625 (6 M KOH at 1 mA cm^{-2})	0.6	94/5000	[36]
3D Co_3O_4–Ag@CNFs	hydrothermal	1880(3 M KOH at 2 A g^{-1})	0.65	NR	[37]
Co_3O_4/C	Solvothermal route	1345(6 M KOH at 1 A g^{-1})	0.8	93/10000	[38]
SnO_x-ZnO/MCNFs composites	electrospinning	783(4 M KOHat 0.5 A g^{-1})	0.5	87/5000	[39]
Co_3O_4/TiO_2/AC	Sol-gel method	946(6 M KOH at 5 mV s^{-1})	0.5	88/2000	[40]
Carbon flakes with $NiCo_2S_4$	hydrothermal	1395(1 M KOH at 1 A g^{-1})	0.6	80/10000	[41]
CuOx@C	hydrothermal	147(3 M KOH at 1 A g^{-1})	0.7	93/10000	[42]
$CuCo_2S_4$/carbon nanotubes	Hydrothermal method	558(2 M KOH at 1 A g^{-1})	0.45	NR	[43]
MnO_2@C	Two-step process	665(6 M KOH at 1 A g^{-1})	1	NR	[44]
Porous carbon-supported Co_3O_4	hydrothermal	516(6 M KOH at 1 A g^{-1})	0.5	94/5000	[45]
NiCo hydroxide/CNT	multi-step process	1896(6 M KOH at 2 A g^{-1})	0.6	NR	[46]
MC @AC	Wet- impregnation	510(1 M Na_2SO_4 at 1 A g^{-1})	1.2	97/5000	This work

Supplementary Table S3. Values of binding energies fitted peaks for MC @AC in Figure 3.

		BE (eV)
Mn $2p_{3/2}$	Mn^{2+}	641.3
	Mn^{3+}	645.3
Mn $2p_{1/2}$	Mn^{2+}	652.6
	Mn^{3+}	656.6
Co $2p_{3/2}$	Co^{2+}	779.9
	Co^{3+}	785.1
Co $2p_{1/2}$	Co^{2+}	795.3
	Co^{3+}	796.2
C 1s	C–C/C=C	284.4
	C–O/C–N	285.7
	C≡O	286.7
	C=O	287.9
O 1s	O^{2-}	530.0
	OH^-	531.4
	H_2O	533.1

SUPPLEMENTARY INFORMATION

Supplementary Table S4. Statistics of C_S of the composite and its components as a function of current density

Current density (A g^{-1})	C_S (F·g^{-1})					
	AC		MC		MC @AC	
	Mean	Standard mean deviation	Mean	Standard mean deviation	Mean	Standard mean deviation
1	144.60	3.97	207.60	2.30	506.00	2.92
2	139.20	4.02	197.00	2.83	503.00	3.08
5	125.60	3.65	186.62	3.16	485.20	3.35
10	113.40	3.91	156.20	4.44	438.00	2.92
15	89.60	4.16	141.80	5.63	394.00	3.94
20	74.20	4.60	117.80	6.06	376.40	4.04

Supplementary Table S5. Results of electrical conductivity measurements of AC, MC, and MC@AC

Electrical conductivity, $\sigma = \frac{t}{RA}$, where t is the thickness of the pellets, R is the bulk resistance and A is the area of the pellets.

	t (cm)	Diameter (cm)	R (Ω)	σ (S cm^{-1}) 10^{-4}
AC	0.154	1.3	130	8.92
MC	0.102	1.3	5000	0.15
MC@AC	0.142	1.3	240	4.45

Supplementary Table S6. Specific surface area, mass-loading, and specific capacitances (gravimetric and areal) of the electrodes

Electrode	BET (m^2/g)	Mass loading(g)	Total surface area (m^2)	Total capacitance (F)	Given current (A)	Areal capacitance (F/m^2)
AC	507	0.0032	1.6224	0.48	0.0032	0.2958
MC	16	0.0026	0.0416	0.546	0.0026	13.125

MC@AC	558	0.0033	1.8414	1.683	0.0033	0.9139

Supplementary Table S7. Fitted charge kinetic parameters

	R_S (Ω)	R_{CT} (Ω)	C_{dl} (mF)	C_p (mF)	Zw (Ω)
AC	1.5	1.5	1.45	_____	1.6
MC	2.2	2.6	1.02	1.36	7.3
MC @AC	1.5	1.6	1.38	1.97	1.9

Supplementary Table S8. Variation of specific energy with specific power of AC//AC and MC @AC// MC @AC

Current density (A g^{-1})	AC//AC		MC @AC// MC @AC	
	Specific power (W kg^{-1})	Specific energy (Wh kg^{-1})	Specific power (W kg^{-1})	Specific energy (Wh kg^{-1})
1	250	8.5	583	30.5
2	500	7.5	1100	29.0
5	1250	7.0	2085	27.8
10	2500	6.7	3710	26.8
15	3750	6.0	4600	25.6
20	4999	5.6	4800	25.0

SUPPLEMENTARY INFORMATION

Supplementary Figure S1: Thermogravimetric analysis of MC@AC. The black curve is thermogravimetric data and the blue curve is its derivative. A weight of 9.3% is determined for MC.

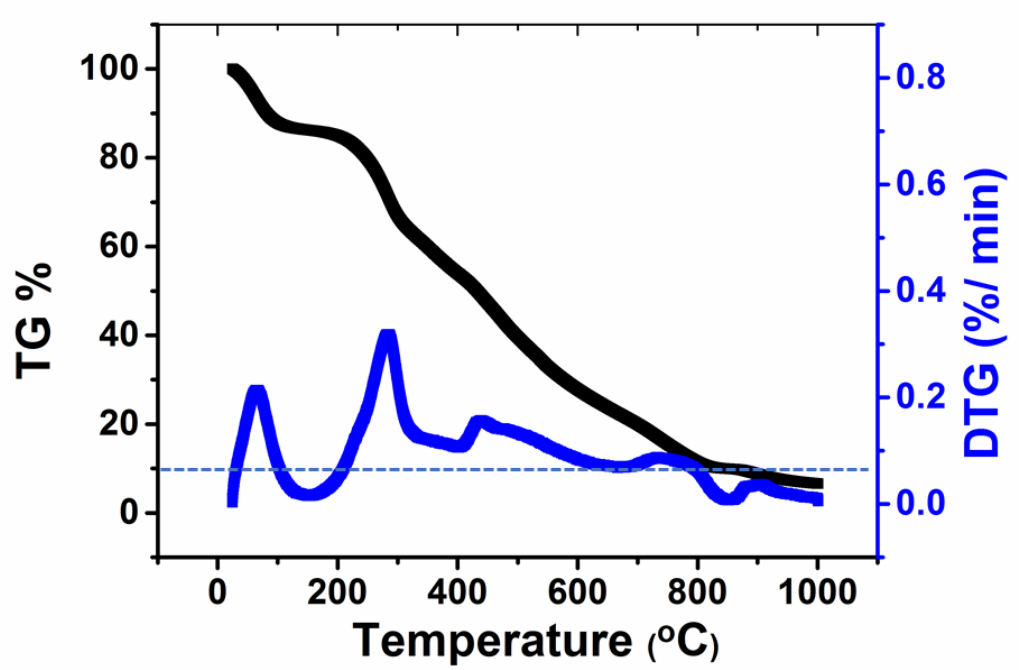

Supplementary Figure S2: FESEM images of (top panel) MC and corresponding EDX results and (bottom panel) MC@AC and corresponding EDX results.

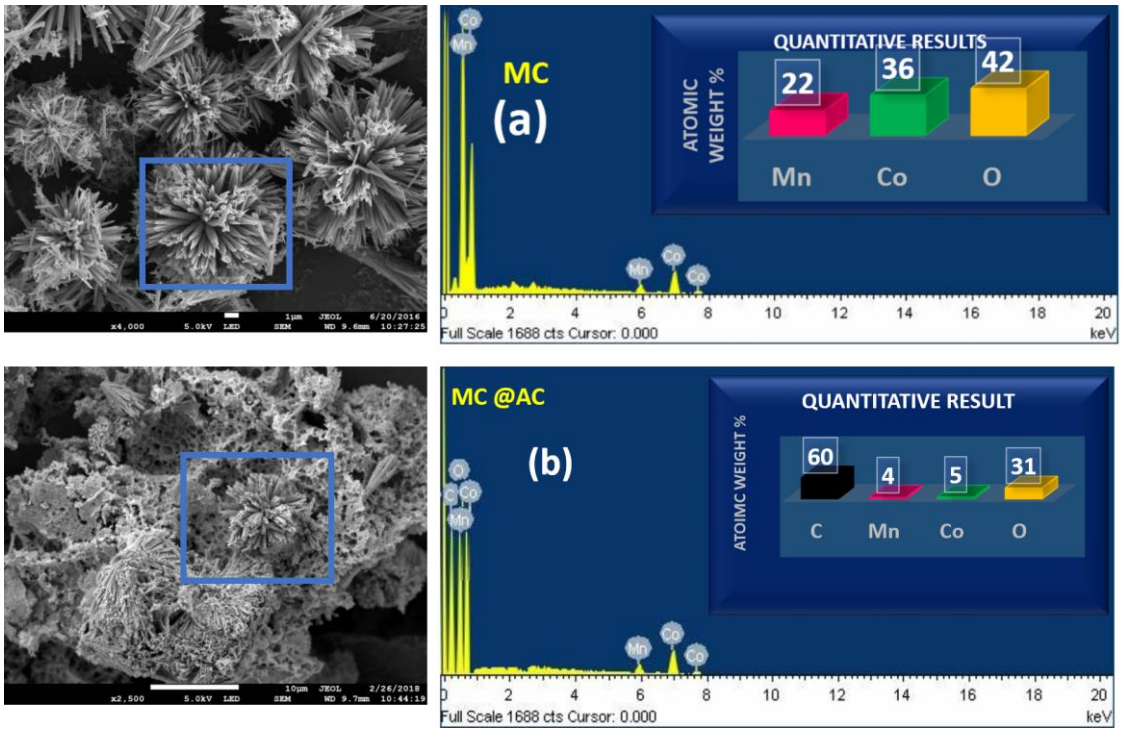

SUPPLEMENTARY INFORMATION

Supplementary Figure S3: FESEM images of MC @AC (a) at 3kx; (b) at 3kx; (c) at 5kx; (d) at 10kx and (e) and (f)TEM images of MC @AC.

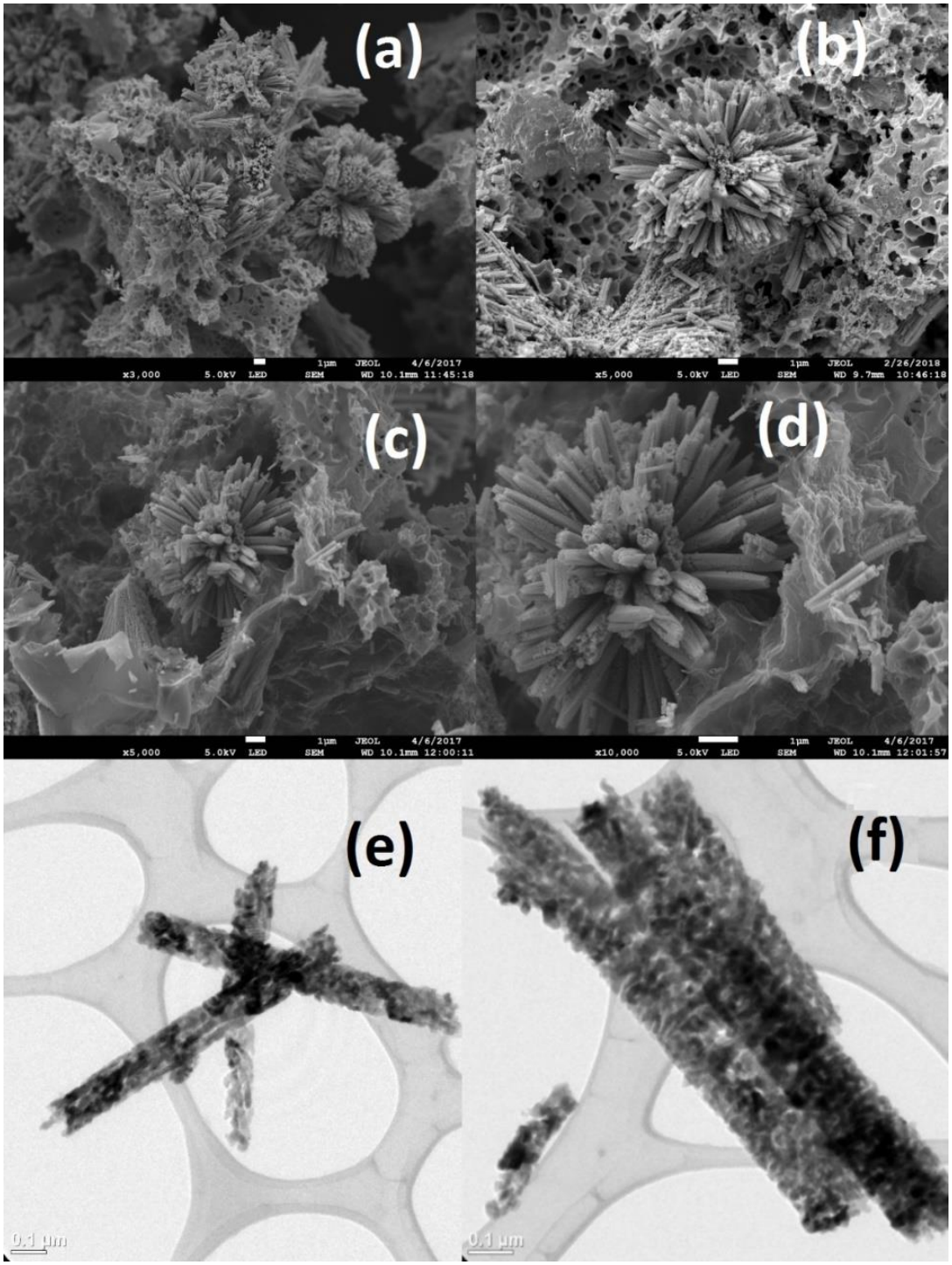

SUPPLEMENTARY INFORMATION

Supplementary Figure S4: Nitrogen adsorption/desorption isotherm for (a)as-synthesized carbon and AC and (b) MC and MC @AC

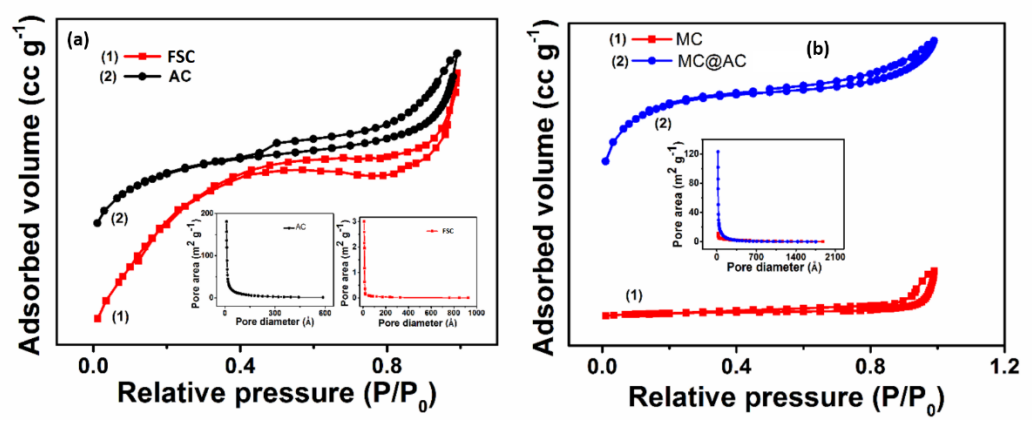

Supplementary Figure S5: Cyclic voltammograms at different scan rates for (a) AC; (b) MC and (c) MC @AC

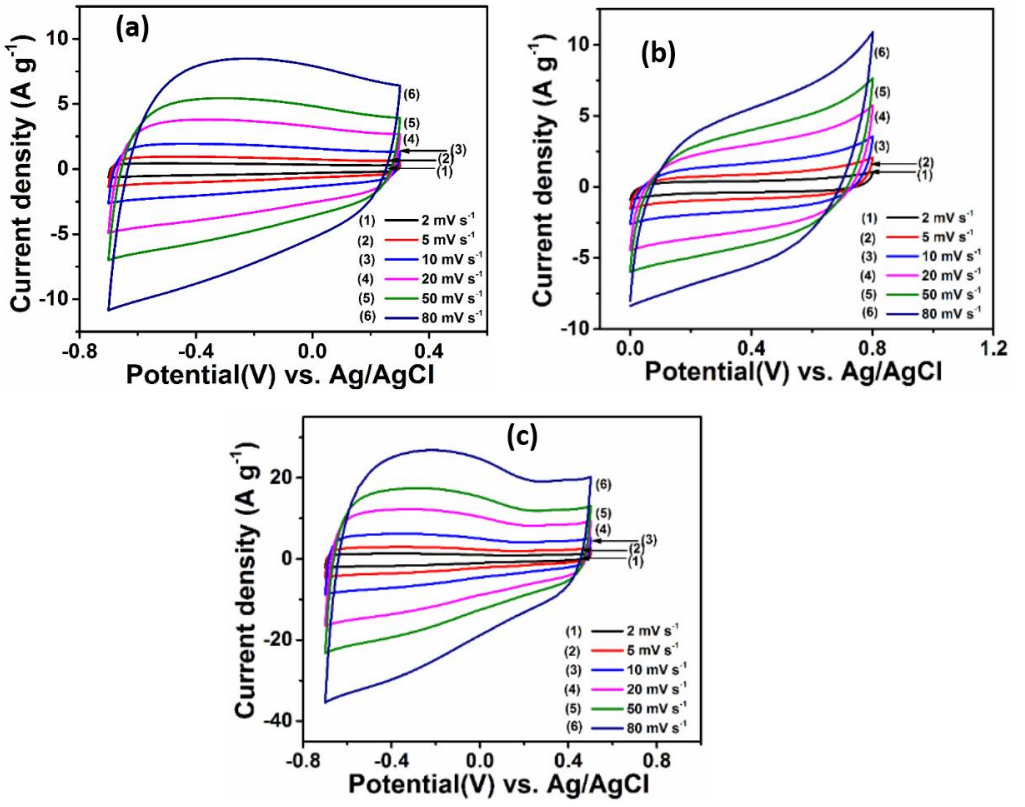

SUPPLEMENTARY INFORMATION

Supplementary Figure S6: EIS spectra of the AC, MC, and MC@AC electrodes, respectively from which ac conductivity was measured. Details of the calculation is in Table S5.

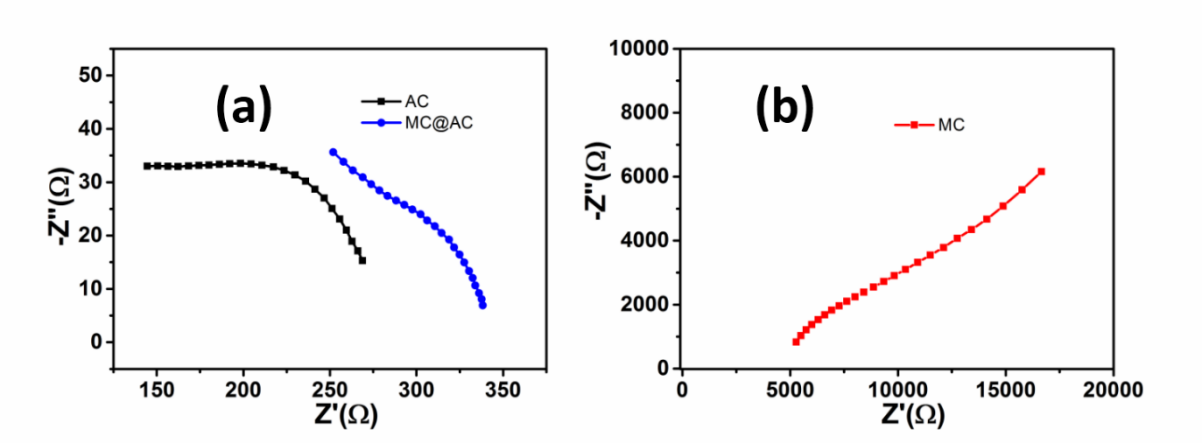

Supplementary Data S1

1. $MnCo_2O_4$ flower (MC)

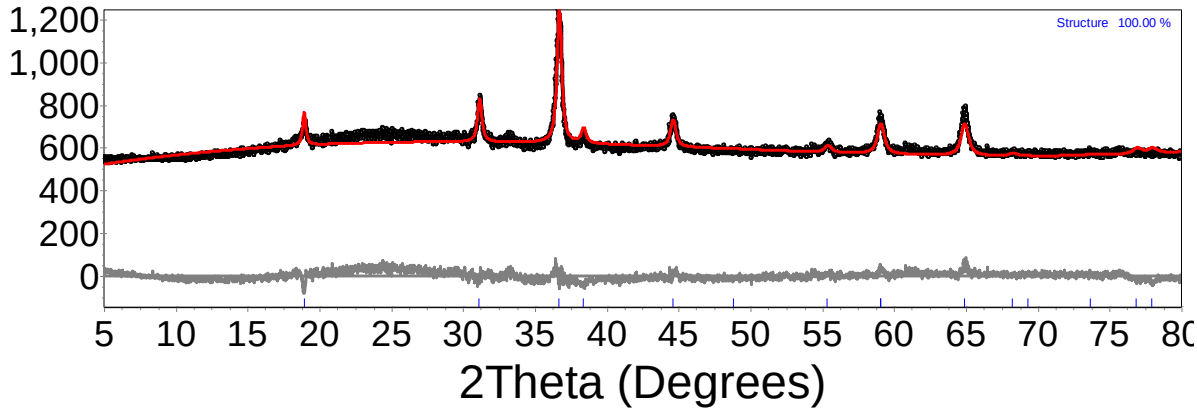

Structure 1

Phase name	Structure
R-Bragg	1.534
Spacegroup	Fd-3m
Scale	1.62222441e-005
Cell Mass	1891.643
Cell Volume (Å^3)	537.07072
Wt% - Rietveld	100.000
Crystallite Size	
Cry Size Lorentzian (nm)	67.4
Cry Size Gaussian (nm)	100.0
Strain	

SUPPLEMENTARY INFORMATION

Strain L	0.5466161
Strain G	0.0001
4 e0	0.13661
Crystal Linear Absorption Coeff. (1/cm)	1312.910
Crystal Density (g/cm^3)	5.849
Lattice parameters	
a (Å)	8.1285015

Site	Np	x	y	z	Atom	Occ	Beq
8a	16	0.12500	0.12500	0.12500	Mn	0.512	0.3497
8a	16	0.12500	0.12500	0.12500	Co	0.4927	-0.05567
16d	8	0.50000	0.50000	0.50000	Co	0.9119	2.407
16d	8	0.50000	0.50000	0.50000	Mn	0.08	1
32e	32	0.36102	0.36102	0.36102	O	1	2.106

---

2. MC @AC

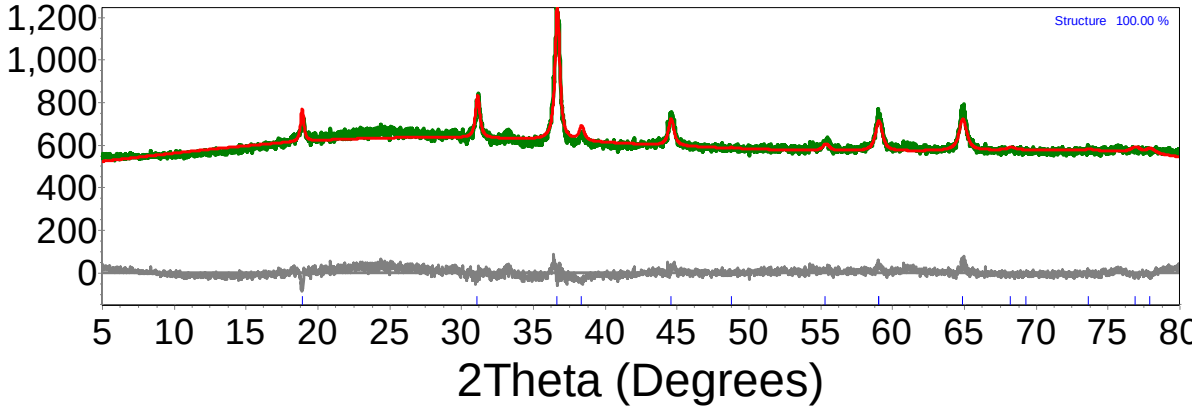

==========

Structure 1

Phase name	Structure
R-Bragg	1.449
Spacegroup	Fd-3m
Scale	1.60365667e-005
Cell Mass	1891.643
Cell Volume (Å^3)	536.98238
Wt% - Rietveld	100.000
Crystallite Size	
Cry Size Lorentzian (nm)	69.4
Cry Size Gaussian (nm)	100.0
Strain	
Strain L	0.5466161
Strain G	0.0001
4 e0	0.13661

SUPPLEMENTARY INFORMATION

Crystal Linear Absorption Coeff. (1/cm) 1313.126
Crystal Density (g/cm^3) 5.850
Lattice parameters
a (Å) 8.1280558

Site	Np	x	y	z	Atom	Occ	Beq
8a	16	0.12500	0.12500	0.12500	Mn	0.512	0.3497
8a	16	0.12500	0.12500	0.12500	Co	0.4927	-0.05567
16d	8	0.50000	0.50000	0.50000	Co	0.9119	2.407
16d	8	0.50000	0.50000	0.50000	Mn	0.08	1
32e	32	0.36102	0.36102	0.36102	O	1	2.106

References

(1) Biswal, M.; Banerjee, A.; Deo, M.; Ogale, S. From dead leaves to high energy density supercapacitors. *Energy & Environmental Science* **2013,** *6* (4), 1249-1259, DOI: 10.1039/C3EE22325F.

(2) Su, X.-L.; Chen, J.-R.; Zheng, G.-P.; Yang, J.-H.; Guan, X.-X.; Liu, P.; Zheng, X.-C. Three-dimensional porous activated carbon derived from loofah sponge biomass for supercapacitor applications. *Applied Surface Science* **2018,** *436*, 327-336, DOI: https://doi.org/10.1016/j.apsusc.2017.11.249.

(3) Kang, X.; Zhu, H.; Wang, C.; Sun, K.; Yin, J. Biomass derived hierarchically porous and heteroatom-doped carbons for supercapacitors. *Journal of Colloid and Interface Science* **2018,** *509* (Supplement C), 369-383, DOI: https://doi.org/10.1016/j.jcis.2017.09.013.

(4) Pourhosseini, S. E. M.; Norouzi, O.; Naderi, H. R. Study of micro/macro ordered porous carbon with olive-shaped structure derived from Cladophora glomerata macroalgae as efficient working electrodes of supercapacitors. *Biomass and Bioenergy* **2017,** *107* (Supplement C), 287-298, DOI: https://doi.org/10.1016/j.biombioe.2017.10.025.

(5) Guo, N.; Li, M.; Sun, X.; Wang, F.; Yang, R. Tremella derived ultrahigh specific surface area activated carbon for high performance supercapacitor. *Materials Chemistry and Physics* **2017,** *201* (Supplement C), 399-407, DOI: https://doi.org/10.1016/j.matchemphys.2017.08.054.

(6) Gong, C.; Wang, X.; Ma, D.; Chen, H.; Zhang, S.; Liao, Z. Microporous carbon from a biological waste-stiff silkworm for capacitive energy storage. *Electrochimica Acta* **2016,** *220* (Supplement C), 331-339, DOI: https://doi.org/10.1016/j.electacta.2016.10.120.

(7) A, D.; Manaf, S. A. B. A.; S, Y.; K, C.; N, K.; Hegde, G. Low cost, high performance supercapacitor electrode using coconut wastes: eco-friendly approach. *Journal of Energy Chemistry* **2016,** *25* (5), 880-887, DOI: https://doi.org/10.1016/j.jechem.2016.08.002.

SUPPLEMENTARY INFORMATION

(8) Wei, L.; Tian, K.; Jin, Y.; Zhang, X.; Guo, X. Three-dimensional porous hollow microspheres of activated carbon for high-performance electrical double-layer capacitors. *Microporous and Mesoporous Materials* **2016,** *227* (Supplement C), 210-218, DOI: https://doi.org/10.1016/j.micromeso.2016.03.015.

(9) Feng, H.; Hu, H.; Dong, H.; Xiao, Y.; Cai, Y.; Lei, B.; Liu, Y.; Zheng, M. Hierarchical structured carbon derived from bagasse wastes: A simple and efficient synthesis route and its improved electrochemical properties for high-performance supercapacitors. *Journal of Power Sources* **2016,** *302* (Supplement C), 164-173, DOI: https://doi.org/10.1016/j.jpowsour.2015.10.063.

(10) Cheng, P.; Gao, S.; Zang, P.; Yang, X.; Bai, Y.; Xu, H.; Liu, Z.; Lei, Z. Hierarchically porous carbon by activation of shiitake mushroom for capacitive energy storage. *Carbon* **2015,** *93* (Supplement C), 315-324, DOI: https://doi.org/10.1016/j.carbon.2015.05.056.

(11) Fuertes, A. B.; Sevilla, M. High-surface area carbons from renewable sources with a bimodal micro-mesoporosity for high-performance ionic liquid-based supercapacitors. *Carbon* **2015,** *94* (Supplement C), 41-52, DOI: https://doi.org/10.1016/j.carbon.2015.06.028.

(12) Wang, D.; Geng, Z.; Li, B.; Zhang, C. High performance electrode materials for electric double-layer capacitors based on biomass-derived activated carbons. *Electrochimica Acta* **2015,** *173* (Supplement C), 377-384, DOI: https://doi.org/10.1016/j.electacta.2015.05.080.

(13) Li, X.; Xing, W.; Zhuo, S.; Zhou, J.; Li, F.; Qiao, S.-Z.; Lu, G.-Q. Preparation of capacitor's electrode from sunflower seed shell. *Bioresource Technology* **2011,** *102* (2), 1118-1123, DOI: https://doi.org/10.1016/j.biortech.2010.08.110.

(14) Ismanto, A. E.; Wang, S.; Soetaredjo, F. E.; Ismadji, S. Preparation of capacitor's electrode from cassava peel waste. *Bioresource Technology* **2010,** *101* (10), 3534-3540, DOI: https://doi.org/10.1016/j.biortech.2009.12.123.

(15) Fan, Y.; Yang, X.; Zhu, B.; Liu, P.-F.; Lu, H.-T. Micro-mesoporous carbon spheres derived from carrageenan as electrode material for supercapacitors. *Journal of Power Sources* **2014,** *268* (Supplement C), 584-590, DOI: https://doi.org/10.1016/j.jpowsour.2014.06.100.

(16) Gao, Y.; Zhang, W.; Yue, Q.; Gao, B.; Sun, Y.; Kong, J.; Zhao, P. Simple synthesis of hierarchical porous carbon from Enteromorpha prolifera by a self-template method for supercapacitor electrodes. *Journal of Power Sources* **2014,** *270* (Supplement C), 403-410, DOI: https://doi.org/10.1016/j.jpowsour.2014.07.115.

(17) Xu, B.; Chen, Y.; Wei, G.; Cao, G.; Zhang, H.; Yang, Y. Activated carbon with high capacitance prepared by NaOH activation for supercapacitors. *Materials Chemistry and Physics* **2010,** *124* (1), 504-509, DOI: https://doi.org/10.1016/j.matchemphys.2010.07.002.

SUPPLEMENTARY INFORMATION

(18) Gong, Y.; Li, D.; Luo, C.; Fu, Q.; Pan, C. Highly porous graphitic biomass carbon as advanced electrode materials for supercapacitors. *Green Chemistry* **2017,** *19* (17), 4132-4140.

(19) Zhang, G.; Chen, Y.; Chen, Y.; Guo, H. Activated biomass carbon made from bamboo as electrode material for supercapacitors. *Materials Research Bulletin* **2018,** *102*, 391-398.

(20) Misnon, I. I.; Zain, N. K. M.; Aziz, R. A.; Vidyadharan, B.; Jose, R. Electrochemical properties of carbon from oil palm kernel shell for high performance supercapacitors. *Electrochimica Acta* **2015,** *174* (Supplement C), 78-86, DOI: https://doi.org/10.1016/j.electacta.2015.05.163.

(21) Luo, X.; Yang, J.; Yan, D.; Wang, W.; Wu, X.; Zhu, Z. MnO_2-decorated 3D porous carbon skeleton derived from mollusc shell for high-performance supercapacitor. *Journal of Alloys and Compounds* **2017,** *723* (Supplement C), 505-511, DOI: https://doi.org/10.1016/j.jallcom.2017.06.215.

(22) Bai, X.; Zhu, W.; Yao, W.; Duan, T. Hydrothermal preparation of CS@MnO_2 with different morphologies for supercapacitor electrode materials. *Materials Letters* **2018,** *210* (Supplement C), 329-332, DOI: https://doi.org/10.1016/j.matlet.2017.09.062.

(23) Zhu, K.; Wang, Y.; Tang, J. A.; Qiu, H.; Meng, X.; Gao, Z.; Chen, G.; Wei, Y.; Gao, Y. In situ growth of MnO2 nanosheets on activated carbon fibers: a low-cost electrode for high performance supercapacitors. *RSC Advances* **2016,** *6* (18), 14819-14825, DOI: 10.1039/C5RA24692J.

(24) Wang, R.; Ma, Y.; Wang, H.; Key, J.; Brett, D.; Ji, S.; Yin, S.; Shen, P. K. A cost effective, highly porous, manganese oxide/carbon supercapacitor material with high rate capability. *Journal of Materials Chemistry A* **2016,** *4* (15), 5390-5394.

(25) Liu, Y.; Cai, X.; Luo, B.; Yan, M.; Jiang, J.; Shi, W. MnO_2 decorated on carbon sphere intercalated graphene film for high-performance supercapacitor electrodes. *Carbon* **2016,** *107*, 426-432, DOI: https://doi.org/10.1016/j.carbon.2016.06.025.

(26) Wang, X.; Fan, X.; Li, G.; Li, M.; Xiao, X.; Yu, A.; Chen, Z. Composites of MnO_2 nanocrystals and partially graphitized hierarchically porous carbon spheres with improved rate capability for high-performance supercapacitors. *Carbon* **2015,** *93*, 258-265, DOI: https://doi.org/10.1016/j.carbon.2015.05.072.

(27) Wu, S.; Hui, K. S.; Hui, K. N. Carbon nanotube@manganese oxide nanosheet core-shell structure encapsulated within reduced graphene oxide film for flexible all-solid-state asymmetric supercapacitors. *Carbon* **2018,** *132*, 776-784, DOI: https://doi.org/10.1016/j.carbon.2017.12.051.

(28) Yuan, C.; Lin, H.; Lu, H.; Xing, E.; Zhang, Y.; Xie, B. Synthesis of hierarchically porous MnO_2/rice husks derived carbon composite as high-performance electrode material for supercapacitors. *Applied Energy* **2016,** *178* (Supplement C), 260-268, DOI: https://doi.org/10.1016/j.apenergy.2016.06.057.

SUPPLEMENTARY INFORMATION

(29) Ma, H.; Weihao, G.; Shenghui, S.; Xinhui, X. Rational fabrication of carbon nanotubes arrays on porous nickel matrix as advanced electrode materials of supercapacitors. *Materials Research Bulletin* **2018,** *105*, 172-177, DOI: https://doi.org/10.1016/j.materresbull.2018.04.040.

(30) Vijayan, B. L.; Misnon, I. I.; Anil Kumar, G. M.; Miyajima, K.; Reddy, M. V.; Zaghib, K.; Karuppiah, C.; Yang, C.-C.; Jose, R. Facile fabrication of thin metal oxide films on porous carbon for high density charge storage. *Journal of Colloid and Interface Science* **2019**, DOI: https://doi.org/10.1016/j.jcis.2019.11.077.

(31) Aruchamy, K.; Nagaraj, R.; Manohara, H. M.; Nidhi, M. R.; Mondal, D.; Ghosh, D.; Nataraj, S. K. One-step green route synthesis of spinel ZnMn2O4 nanoparticles decorated on MWCNTs as a novel electrode material for supercapacitor. *Materials Science and Engineering: B* **2020,** *252*, 114481, DOI: https://doi.org/10.1016/j.mseb.2019.114481.

(32) Sun, H.; Pan, J.; Yan, X.; Shen, W.; Zhong, W.; Cheng, X. MnO2 nanoneedles loaded on silicon oxycarbide-derived hierarchically porous carbon for supercapacitor electrodes with enhanced electrochemical performance. *Ceramics International* **2019,** *45* (18, Part A), 24802-24810, DOI: https://doi.org/10.1016/j.ceramint.2019.08.222.

(33) Cui, L.; Cheng, C.; Peng, F.; Yang, Y.; Li, Y.; Jia, M.; Jin, X. A ternary MnO2-deposited RGO/lignin-based porous carbon composite electrode for flexible supercapacitor applications. *New Journal of Chemistry* **2019,** *43* (35), 14084-14092, DOI: 10.1039/C9NJ02184A.

(34) Nagamuthu, S.; Ryu, K.-S. MOF-derived microstructural interconnected network porous Mn2O3/C as negative electrode material for asymmetric supercapacitor device. *CrystEngComm* **2019,** *21* (9), 1442-1451, DOI: 10.1039/C8CE01683F.

(35) Xu, L.; Zhang, L.; Cheng, B.; Yu, J. Rationally designed hierarchical NiCo2O4–C@Ni(OH)2 core-shell nanofibers for high performance supercapacitors. *Carbon* **2019,** *152*, 652-660, DOI: 10.1016/j.carbon.2019.06.062.

(36) Sajjad, M.; Jiang, Y.; Guan, L.; Chen, X.; Iqbal, A.; Zhang, S.; Ren, Y.; Zhou, X.; Liu, Z. NiCo2S4 nanosheet grafted SiO2@C core-shelled spheres as a novel electrode for high performance supercapacitors. *Nanotechnology* **2019,** *31* (4), 045403, DOI: 10.1088/1361-6528/ab4d0a.

(37) Mukhiya, T.; Dahal, B.; Ojha, G. P.; Chhetri, K.; Lee, M.; Kim, T.; Chae, S.-H.; Tiwari, A. P.; Muthurasu, A.; Kim, H. Y. Silver nanoparticles entrapped cobalt oxide nanohairs/electrospun carbon nanofibers nanocomposite in apt architecture for high performance supercapacitors. *Composites Part B: Engineering* **2019,** *178*, 107482, DOI: https://doi.org/10.1016/j.compositesb.2019.107482.

(38) Yin, Q.; He, L.; Lian, J.; Sun, J.; Xiao, S.; Luo, J.; Sun, D.; Xie, A.; Lin, B. The synthesis of Co3O4/C composite with aloe juice as the carbon aerogel substrate for asymmetric supercapacitors. *Carbon* **2019,** *155*, 147-154, DOI: https://doi.org/10.1016/j.carbon.2019.08.060.

SUPPLEMENTARY INFORMATION

(39) Liu, J.; Xu, T.; Sun, X.; Bai, J.; Li, C. Preparation of stable composite porous nanofibers carried SnOx-ZnO as a flexible supercapacitor material with excellent electrochemical and cycling performance. *Journal of Alloys and Compounds* **2019,** *807*, 151652, DOI: https://doi.org/10.1016/j.jallcom.2019.151652.

(40) Sirengo, K.; Jande, Y. A. C.; Kibona, T. E.; Hilonga, A.; Muiva, C.; King'ondu, C. K. Fish bladder-based activated carbon/Co3O4/TiO2 composite electrodes for supercapacitors. *Materials Chemistry and Physics* **2019,** *232*, 49-56, DOI: https://doi.org/10.1016/j.matchemphys.2019.04.059.

(41) Liu, Y.; Li, Z.; Yao, L.; Chen, S.; Zhang, P.; Deng, L. Confined growth of NiCo2S4 nanosheets on carbon flakes derived from eggplant with enhanced performance for asymmetric supercapacitors. *Chemical Engineering Journal* **2019,** *366*, 550-559, DOI: https://doi.org/10.1016/j.cej.2019.02.125.

(42) Wang, Q.; Zhang, Y.; Xiao, J.; Jiang, H.; Hu, T.; Meng, C. Copper oxide/cuprous oxide/hierarchical porous biomass-derived carbon hybrid composites for high-performance supercapacitor electrode. *Journal of Alloys and Compounds* **2019,** *782*, 1103-1113, DOI: https://doi.org/10.1016/j.jallcom.2018.12.235.

(43) Li, H.; Li, Z.; Wu, Z.; Sun, M.; Han, S.; Cai, C.; Shen, W.; Liu, X.; Fu, Y. Enhanced electrochemical performance of CuCo2S4/carbon nanotubes composite as electrode material for supercapacitors. *Journal of Colloid and Interface Science* **2019,** *549*, 105-113, DOI: https://doi.org/10.1016/j.jcis.2019.04.056.

(44) Xie, Y.; Yang, C.; Chen, P.; Yuan, D.; Guo, K. MnO2-decorated hierarchical porous carbon composites for high-performance asymmetric supercapacitors. *Journal of Power Sources* **2019,** *425*, 1-9, DOI: https://doi.org/10.1016/j.jpowsour.2019.03.122.

(45) Xiao, S.; Huang, J.; Lin, C.; Xie, A.; Lin, B.; He, L.; Sun, D. Porous carbon derived from rice husks as sustainable bioresources: Insights into the role of micro/mesoporous hierarchy in Co3O4/C composite for asymmetric supercapacitors. *Microporous and Mesoporous Materials* **2020,** *291*, 109709, DOI: https://doi.org/10.1016/j.micromeso.2019.109709.

(46) Zhou, Q.; Fan, T.; Li, Y.; Chen, D.; Liu, S.; Li, X. Hollow–structure NiCo hydroxide/carbon nanotube composite for High–Performance supercapacitors. *Journal of Power Sources* **2019,** *426*, 111-115, DOI: https://doi.org/10.1016/j.jpowsour.2019.04.035.